Easily-Accessible Human Skin-Fat-Muscle Phantoms for Dependable *In-Vitro* Testing of Biomedical Devices

Yonghee Chang*, Naveed Ahmed* and Kaiyuan Yang

***Abstract*— Human phantoms are a viable alternative for *in-vitro* biomedical device testing, replacing conventional animal tissues and liquid solutions that compromise reproducibility and accuracy. This paper reports a novel human phantom design framework that accurately replicates the electrical properties of human skin, fat, and muscle, using easily accessible and low-cost materials and simple fabrication processes. These phantoms cover an important frequency range of 100 kHz to 50$^+$ MHz, which is widely used for wearable and implantable biomedical devices and yet undiscovered. Through a set of electrical, mechanical, and long-term stability measurements, the proposed phantoms demonstrate superior practicality and accuracy for *in-vitro* testing than existing approaches.**

I. Introduction

Wearable and implantable biomedical devices have gained increasing attention as technology enablers for revolutionary bioelectronic medicine [1] and digital health applications. Wireless technologies, such as inductive and intra-body coupling, facilitate untethered data and power transmission to these devices, which are essential to their miniaturization, comfort, and acceptance by the public. During the research and development of these wireless systems, the *in-vitro* test is an essential step to study and assure the system's performance, reliability, and safety before *in-vivo* tests.

Animal tissues, such as porcine, is the most common option for *in-vitro* testing of biomedical devices [2]. Although animal tissues have a similar composition as human tissues and are readily available, they differ in electrical properties and structure. Additionally, their organic nature, irregular shape, and susceptibility to water loss during freeze-thaw cycles for storage present challenges for long-term use. On the other hand, solutions such as phosphate-buffered saline (PBS) have been an alternative with good longevity, which is much easier to manage and reproduce experimental results compared to animal tissues [3]. However, as a liquid solution, PBS does not replicate the structural and material properties of human tissue, yielding much lower testing accuracy. To overcome these limitations, hydrous phantoms that mimic human tissue have been proposed [4]–[7]. These phantoms offer great flexibility in customizing properties and structures and are easy to store and reuse. However, several challenges remain in prior works.

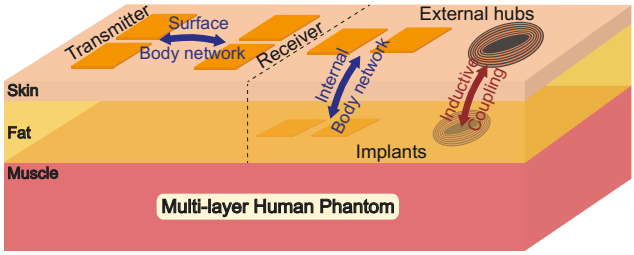

Fig. 1. Multi-layer human skin-fat-muscle phantoms for *in-vitro* testing of wearable and implantable biomedical devices.

A high-quality phantom should not only replicate dielectric properties of human tissue across the desired frequency range, but also be readily accessible, durable, and support multi-layer structures, e.g. skin, fat, and muscle, to better emulate human tissues and enhance the fidelity of *in-vitro* testing. Existing phantom designs have three primary limitations. First, they focus on either GHz or narrow frequency ranges in the MHz regime, where matching is easier due to the flatness of electrical properties [4], [5], [7]. However, many wireless technologies work in the hundreds of kHz to hundreds of MHz range [8] and we are not aware of any phantom covering this frequency range in the literature. Second, they lack multi-layer structures, longevity, and dynamic mechanical property [6] evaluations critical for practical applications. Third, they rely on exotic or proprietary materials, such as TX151 [4], [5] and ATO/TIO_2 [7].

Here, we report a novel framework for synthesizing human phantoms that accurately replicate human skin, fat, and muscle, as shown in Fig. 1. In addition to matching the electrical properties of human tissues, we focus our efforts on using easily accessible ingredients (kaolin and magnesium chloride) to facilitate the adoption of our phantom. The phantoms are designed to match the relative permittivity (ε_r) and conductivity (σ) over a wide frequency range from 100 kHz to 50$^+$ MHz[1], which covers the common spectrum utilized for wireless biomedical technologies, but unexplored in previous phantom design efforts. We further demonstrate that our phantoms can be easily shaped and assembled to create multi-layer structures that better mimic real human and animal tissues. Last but not least, we comprehensively evaluated the long-term usability and mechanical properties of the phantoms to demonstrate their practicality.

* These authors contributed equally to the work.

This work is supported in part by the National Science Foundation (NSF) under Grant No. 2146476.

Y. Chang and K. Yang are with the Department of Electrical and Computer Engineering, Rice University, Houston, TX, USA (e-mail: yc155@rice.edu and kyang@rice.edu)

N. Ahmed is with the Department of Electrical and Computer Engineering, University of Texas at Austin, Austin, TX, USA (e-mail: naveed.ahmed@utexas.edu)

[1]We add a $^+$ notation to the reported frequency upper bound as it is limited by the bandwidth of our impedance analyzer (Bode100).

II. Phantom design and fabrication

A. Design principles

An ideal phantom must meet the physical and dielectric requirements simultaneously. The selection of an appropriate base material is a critical step in phantom design, as it sets the foundation of dielectric properties. Subsequent addition of control materials allows further tuning of these dielectric properties to meet specific requirements. Meanwhile, we emphasize the importance of having easily accessible and easy-to-use materials to facilitate the adoption of phantoms.

Agar, gelatin, and TX-151 are common base materials for achieving the structural integrity of the phantom [4]–[7]. However, solely relying on agar or gelatin may result in insufficient solidification or require excessive quantities, complicating the tuning of the phantom's electrical properties with control materials. Moreover, while the physical properties of TX-151 make it suitable for phantoms, its limited availability and proprietary nature motivate us to find a more accessible substitute for practical phantom production [9]. To overcome these limitations, we propose a combination of agar and kaolin, a type of clay, for the skin phantom and agar mixed with gelatin for the muscle phantom. Additionally, the use of kaolin improves the longevity of the phantom by mitigating water loss over time [10], a prevalent issue with conventional recipes.

To emulate human tissues for *in-vitro* testing of biomedical devices, two key dielectric properties must be matched: relative permittivity (ε_r) and conductivity (σ). These properties are controlled by the addition of control materials, such as chlorides. The use of chloride allows for a notable increase in σ in the phantom, with an equally significant increase in ε_r [11]. We substituted traditional sodium chloride with magnesium chloride because the latter's weaker ionic bonds [12] allows the adjustment of σ with less impact on ε_r. The use of sodium chloride also deteriorates water retention as a result of the anti-salt characteristics of the sulfate groups in agar [13]. Magnesium chloride solves this issue as the weaker ionic bonds are rejected less intensely, leading to a longer-lasting recipe. Similarly, the use of kaolin allows for a smoother increase in the σ suitable for phantoms that necessitate lower conductivity levels, e.g., skin. With pure agar or gelatin phantoms, σ follows a powered function of frequency as water becomes the dominant dielectric material [14]. The addition of kaolin, a polar molecule, breaks this powered dependency and makes the conductivity of the phantom relatively flat over frequencies.

TABLE I
Phantom recipes

Phantom	Material	Percentage (%)
Skin	Deionized Water	90.0
	Agar	5.0
	Kaolin	5.0
Muscle (Z)	Deionized Water	91.7
	Agar	2.7
	Gelatin	5.4
	Magnesium Chloride	0.2
Muscle (σ)	Deionized Water	91.7
	Agar	2.6
	Gelatin	5.3
	Magnesium Chloride	0.4
Muscle (ε_r)	Deionized Water	95.0
	Gelatin	5.0
Fat	Deionized Water	12.5
	Refined Coconut Oil	51.9
	Flour	6.7
	Sodium Hydroxide	28.9

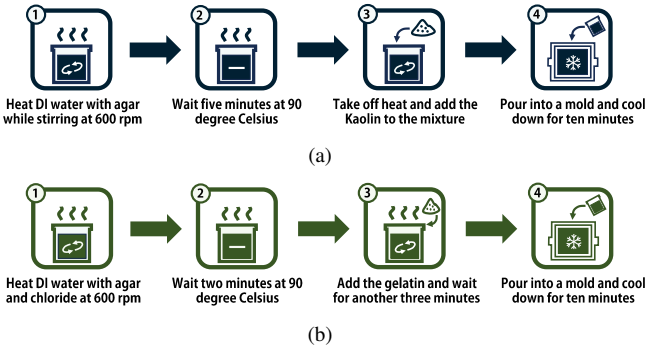

Fig. 2. Fabrication procedure of (a) skin and (b) muscle phantoms.

Among the three phantoms, the muscle is most challenging as it requires high σ and relatively low ε_r at the same time, due to β-dispersion in the 1 MHz range [7]. This requirement contrasts with the effect of chloride. To overcome this challenge, we propose to match the parallel impedance (Z) instead, which is especially useful for testing intra-body and near-field coupling. The impedance calculation is derived from the parallel RC tissue model [15]. Designing a Z-matching phantom becomes less challenging as the effects of ε_r and σ are lumped into a single impedance value.

B. Proposed phantom design and fabrication

Our phantom recipes that successfully mimic the skin, fat, and muscle layers of human tissue are presented in Table I. For the agar-based skin phantom, we incorporated kaolin to increase viscosity and σ without excessively increasing the ε_r typically associated with chloride-based solutions. For the oil-based fat phantom, we utilized refined coconut oil and flour to effectively lower the dielectric constant while ensuring solidification, with small amounts of water and sodium hydroxide to facilitate thorough mixing [4]. For the gelatin-based muscle phantom, addressing the complexity of replicating muscle tissue necessitated the creation of three distinct formulas. These include a gelatin-only phantom matching muscle ε_r and two others for matching σ and Z, respectively, both of which are based on gelatin and agar mixtures. The latter two are designed to achieve proper solidification while minimizing the amount of solidifying agents and incorporating magnesium chloride to increase σ with minimal impact on ε_r. The reduction of solidification agents allows for precise adjustments in ε_r and σ, without sacrificing physical properties.

Our phantoms are fabricated with simple laboratory equipment, including a magnetic stirrer, a hot plate, a scale accurate to the hundredth of a gram, and glassware. The skin

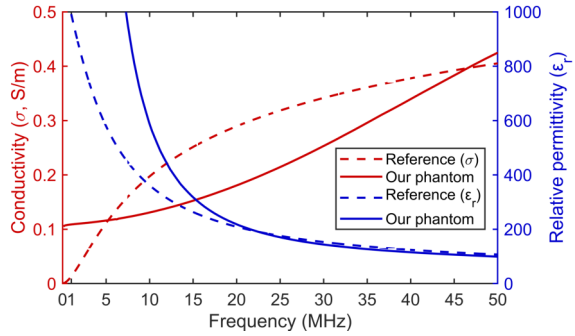

(a)

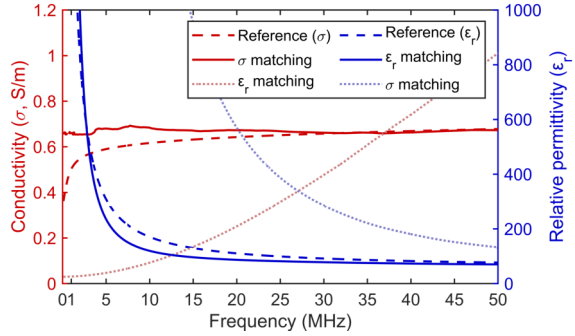

(b)

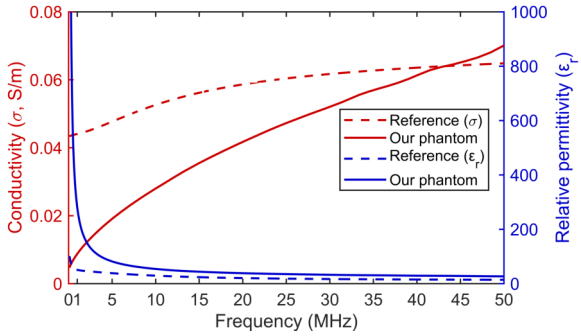

(c)

Fig. 3. Conductivity (red-σ) and permittivity (blue-ε_r) measurement results of individual layers: (a) skin, (b) muscle with both ε_r and σ matching phantoms, and (c) fat along with their references.

and muscle phantoms share similar fabrication procedures with minor adjustments in key materials, as depicted in Fig. 2. The fat layer follows a distinct procedure for creating a non-hydrous phantom. First, water and sodium hydroxide are thoroughly mixed, taking care to avoid splashing. Then, refined oil and flour are quickly added to the mixture, using the heat from the sodium hydroxide dissolution. All three phantoms must be cooled for ten minutes or until completely solid, upon which the dielectric properties will cease temperature-dependent drifting.

III. Measurement

A. Property matching of individual layers

To evaluate the precision of our phantom against the reference data from the IT'IS database [16], we measured the dielectric properties of each phantom. For this measurement,

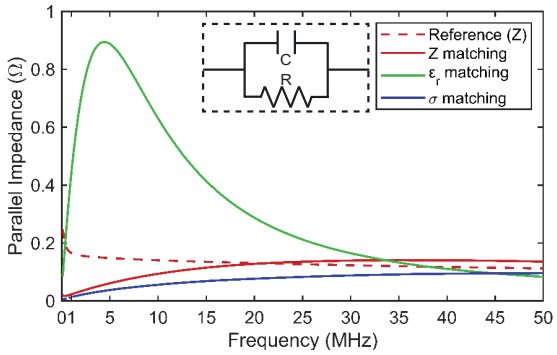

Fig. 4. Calculated parallel impedance of the measured Z (red), ε_r (green), and σ (blue) matching phantoms along with the reference.

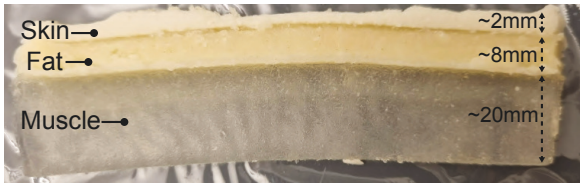

Fig. 5. Cross-section view of the fabricated multi-layer phantom.

a 10 cm copper pipe, rod, and plastic caps were used with an impedance analyzer (Bode100) to create a coaxial probe. This setup allowed us to measure the conductance and capacitance of the filler between the pipe and rod, from which ε_r and σ were extracted based on the Eq. (1) and (2), where L is the length of pipe, r_{a} is the radius of rod, and r_{b} is the radius of pipe.

$$\varepsilon_{r.filler} = \frac{C_{measure} \times \ln(\frac{r_b}{r_a})}{2\pi\varepsilon_0 L} \tag{1}$$

$$\sigma_{filler} = \frac{G_{measure} \times \ln(\frac{r_b}{r_a})}{2\pi L} \tag{2}$$

Fig. 3 illustrates the measured dielectric properties of the skin muscle, and fat phantoms. In general, at lower frequencies, we observed that the relative ε_r is highly sensitive to frequency changes. In contrast, at higher frequencies, this sensitivity diminishes, leading to a higher matching accuracy in this range. Fig. 3 (b) displays two distinct phantoms, each modified to match either the σ or ε_r of muscle. The results indicate that the phantom designed for σ is better suited for higher frequencies, whereas the phantom tailored for ε_r demonstrates optimal performance at lower frequencies. Fig. 4 shows the parallel impedance of three distinct muscle phantoms. Among these, the Z-matching phantom performs better in aligning with the reference parallel impedance.

B. Multi-layer phantoms

We fabricated a $10cm \times 10cm \times 3cm$ multi-layer phantom designed to replicate skin, fat, and muscle layers, assembling each layer sequentially within a 3D printed PLA box. This phantom is composed of a skin layer of 2 mm, a fat layer of 8 mm, and a muscle layer of 20 mm, as depicted in Fig. 5. Using this multi-layered structure, we studied two distinct

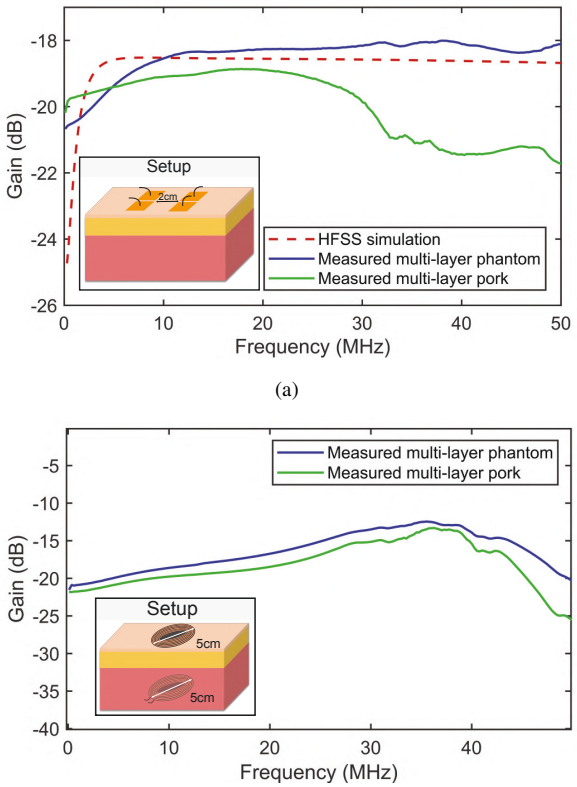

Fig. 6. Channel measurement using multi-layer phantoms and other references for (a) wearable galvanic coupling and (b) implantable inductive coupling applications.

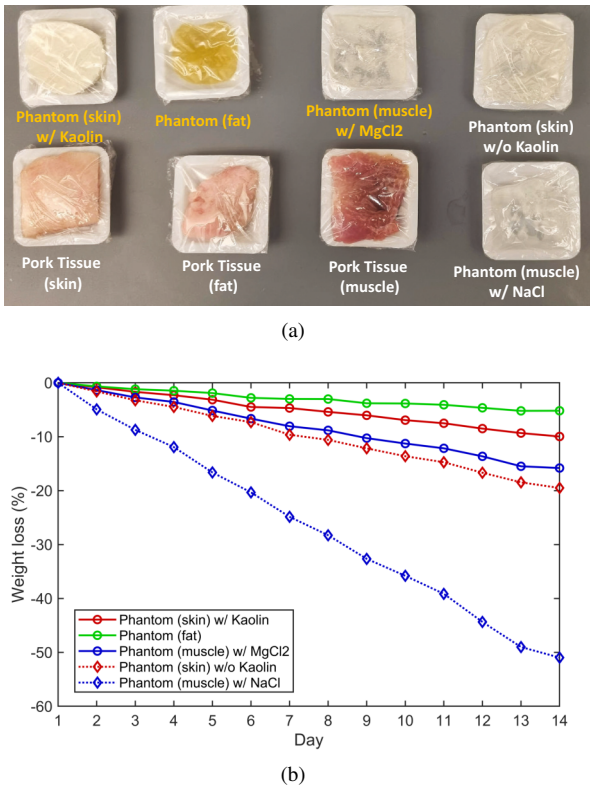

Fig. 7. (a) Eight samples and (b) their weight losses over two weeks.

use cases, wearable galvanic coupling (with two pairs of 2 cm by 2 cm electrodes) and implantable inductive coupling (a pair of 5 cm diameter circular coils), by measuring the channel characteristics (S21) using Bode100.

In galvanic coupling tests, as shown in Fig. 6 (a), the channel gain and bandwidth measured with our phantom tracks the HFSS simulation based on IT'IS dataset [16] significantly better than multi-layer pork. In the inductive measurements shown in Fig. 6 (b), the phantom matches well with the multi-layer pork, proving the effectiveness of the phantom for testing inductive links. The close match between our phantom and pork results in the inductive test eliminates the need for a reference, unlike the galvanic test. These measurements are limited to 50 MHz due to the bandwidth of our instrument, but the trends shown in Fig. 6 suggest the possibility of using our phantom at higher frequencies.

C. Long-term stability

To test the long-term stability of each added material, we prepared eight samples, including fresh porcine tissues, shown in Fig. 7 (a). After preparing the samples, we applied moldicide to all samples, sealed them with plastic wrap, and stored them in normal room conditions. We measured the samples' weight loss over fourteen consecutive days as an indicator of their longevity, since water loss is directly related to changes in dielectric properties, excluding other changes in composition [17]. As expected, all porcine samples developed mold after only a few days, rendering them unusable for testing as molds drastically change the properties of the tissue. As displayed in Fig. 7 (b), the addition of kaolin doubled the life span of the pure agar sample, while the substitution of sodium chloride with magnesium chloride quadrupled the life span of the muscle phantom. As such, kaolin and magnesium chloride-based phantoms prove to be superior for long-term electrical testing than animal tissues and prior phantom designs.

D. Mechanical properties

We measured the mechanical properties of three samples (pure agar, gelatin-agar, and kaolin-agar) using an ARES G2 Rheometer to assess solidification performance. Specifically, we analyzed the phantom's dynamic modulus (storage and loss) similarly to typical soft tissue measurements [18]. As illustrated in Fig. 8 (a) and (b), the agar-gelatin combination for muscle exhibited a higher dynamic modulus and viscosity, indicating a better solidification performance compared to pure agar. Similarly, the agar-kaolin blend also demonstrated enhanced performance relative to pure agar, thereby proving the effect of kaolin in solidification.

E. Comparison with related works

A comparison table among our design and prior arts is detailed in Table II. We introduce a Figure of Merit (FoM) to describe the matching accuracy between phantom and reference, considering the dynamic range of the frequency band it supports. The FoM is calculated by dividing the matching

TABLE II

COMPARISON TO THE STATE-OF-THE-ART

Phantom Evaluation		This Work	EMBC'16 [4]	COMCAS'17 [5]	EMBC'19 [6]	EMBC'21 [7]
Frequency range		100kHz-50^{+}MHz	30-200MHz	1-2GHz	20Hz-100kHz	100kHz-1MHz
FoM (ε_r/σ)	Skin	16%/20%	247%/N/A	8%/73%	N/A for both	N/A for both
	Muscle	17%/7%	29%/N/A	3%/77%	19%/51% and 23%/19%	3%/20%
Key Materials		Kaolin and $MgCl_2$	TX151	TX151 and HEC	Aluminum and Glycine	ATO/TIO_2
Ease of Access		Easy to access	Hard to access	Hard to access	Easy to access	Hard to access
Longevity		2-weeks (room temperature)	N/A	N/A	1-week	N/A
Multi-layer		Available and evaluated	Available	Available	N/A	N/A
Physical Properties		Dynamic modulus and viscosity	N/A	N/A	Young's modulus	N/A

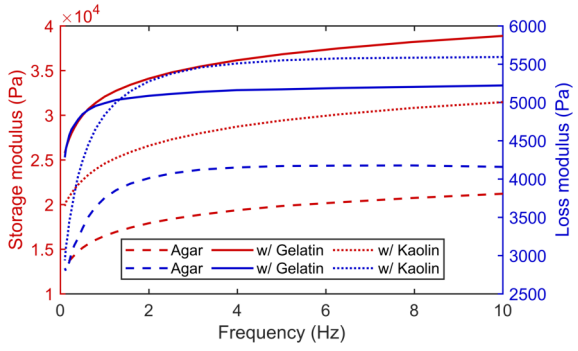

(a)

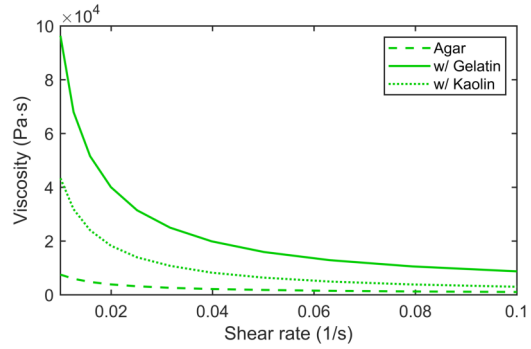

(b)

Fig. 8. Measured mechanical properties: (a) storage and loss modulus between 0.1-10 Hz and (b) viscosity between 0.01-0.1 s^{-1}.

errors' quadratic mean (RMS) by the dynamic range of its frequency in the dB scale. The matching errors are sampled on a log scale, including starting and ending points. A lower FoM value indicates better matching properties.

IV. CONCLUSIONS

We present a framework for producing human phantoms that accurately mimic the electrical properties of human skin, fat, and muscle using materials that are easy to access and use. The incorporation of kaolin in the skin layer aids in solidification, ensuring better dielectric property matching and longevity. Substituting magnesium chloride for sodium chloride enhances the longevity and the matching of dielectric properties. The results of single and multi-layer tests demonstrate high accuracy in matching references. The mechanical property and long-term durability tests further establish the advantages of using the presented phantoms for *in-vitro* testing of wearable and implantable devices.

REFERENCES

[1] H. C. Koydemir et al., "Wearable and implantable sensors for biomedical applications," Annual Review of Analytical Chemistry, vol. 11, no. 1, pp. 127–146, 2018.

[2] Y. Chang et al., "Seamless capacitive body channel wireless power transmission toward freely moving multiple animals in an animal cage," IEEE Transactions on Biomedical Circuits and Systems, vol. 16, no. 4, pp. 714–725, 2022.

[3] Z. Zhao et al., "Ionic communication for implantable bioelectronics". Science Advances, vol. 8, no. 14, 2022.

[4] L. Fomundam and J. Lin, "Multi-layer low frequency tissue equivalent phantoms for noninvasive test of shallow implants and evaluating antenna-body interaction," 2016 38th Annual International Conference of the IEEE Engineering in Medicine and Biology Society (EMBC), 2016, pp. 2353-2356.

[5] Q. Bonds and T. Weller, "Multi-layer RF tissue phantoms for mimicking a human core," 2017 IEEE International Conference on Microwaves, Antennas, Communications and Electronic Systems (COMCAS), 2017, pp. 1-4.

[6] Y. Yu, A. Lowe, G. Anand and A. Kalra, "Tissue phantom to mimic the dielectric properties of human muscle within 20 Hz and 100 kHz for biopotential sensing applications," 2019 41st Annual International Conference of the IEEE Engineering in Medicine and Biology Society (EMBC), 2019, pp. 6490-6493.

[7] S. Toyoda, T. Yamamoto and K. Koshiji, "Prototype and evaluation of high-hydrous gel phantom for 100 kHz to 1 MHz using ATO/TiO2," 2021 43rd Annual International Conference of the IEEE Engineering in Medicine & Biology Society (EMBC), 2021, pp. 6814-6817.

[8] V. Nair et al., "Miniature battery-free bioelectronics". Science, vol. 382, no. 6671, 2023.

[9] Oil Center Research, L.L.C., https://oilcenter.com/product/tx-151/

[10] B. Zhang et al., "Effect of kaolin content on the performances of kaolin-hybridized soybean meal-based adhesives for wood composites," Composites Part B: Engineering, vol. 173, p. 106919, 2019.

[11] D. Bennett, "NaCl doping and the conductivity of agar phantoms," Materials Science and Engineering: C, vol. 31, no. 2, pp. 494–498, 2011.

[12] M. J. Martins et al., "Solubility of different salts used in the control of the water activity of foods," Ciência e Agrotecnologia, vol. 47, 2023.

[13] J. Muthukumar, R. Chidambaram, and S. Sukumaran, "Sulfated polysaccharides and its commercial applications in Food Industries—a review," Journal of Food Science and Technology, vol. 58, no. 7, pp. 2453–2466, 2020.

[14] V. V. Shcherbakov, V. I. Ermakov, and Yu. M. Artemkina, "Dielectric characteristics of water and electric conductivity of aqueous electrolytes," Russian Journal of Electrochemistry, vol. 53, no. 12, pp. 1301–1306, 2017.

[15] D. J. Bora and R. Dasgupta, "Estimation of skin impedance models with experimental data and a proposed model for human skin impedance," IET Systems Biology, vol. 14, no. 5, pp. 230–240, 2020.

[16] Hasgall PA, Di Gennaro F, Baumgartner C, Neufeld E, Lloyd B, Gosselin MC, Payne D, Klingenböck A, Kuster N, "IT'IS Database for thermal and electromagnetic parameters of biological tissues," itis.swiss/database, Version 4.1, Feb 22, 2022.

[17] C. Mendes and C. Peixeiro, "Fabrication, measurement and time decay of the electromagnetic properties of semi-solid water-based Phantoms," Sensors, vol. 19, no. 19, p. 4298, 2019.

[18] A. B., S. Rao, and H. J. Pandya, "Engineering approaches for characterizing soft tissue mechanical properties: A Review," Clinical Biomechanics, vol. 69, pp. 127–140, 2019.